

Evolution of the local structure at the phase transition in CeO₂-Gd₂O₃ solid solutions

A. Kossoy,^{1,*} Q. Wang,² R. Korobko,¹ V. Grover,³ Y. Feldman,⁴ E. Wachtel,¹ A. K. Tyagi,³ A. I. Frenkel,^{2,†} and I. Lubomirsky^{1,‡}

¹*Department of Materials and Interfaces, Weizmann Institute of Science, Rehovot, Israel*

²*Physics Department, Yeshiva University, 245 Lexington Avenue, New York, New York 10016, USA*

³*Chemistry Division, Bhabha Atomic Research Center, Mumbai, India*

⁴*Chemical Research Support Unit, Weizmann Institute of Science, Rehovot, Israel*

(Received 14 May 2012; revised manuscript received 8 December 2012; published 4 February 2013)

We investigated the local environment of the Ce and Gd ions in one of the most important oxygen ion conductors, the CeO₂-Gd₂O₃ solid solution, using L_{III} edge extended x-ray absorption fine structure (EXAFS) spectroscopy and x-ray absorption near edge spectroscopy (XANES). The average Gd-O distance, as deduced by EXAFS, decreases gradually with increasing Gd content, whereas a sharp decrease in the average Ce-O distance occurs at 25 mol% Gd, accompanying the appearance of structural features characteristic of double fluorite symmetry. An abrupt change in the local environment of Ce, rather than of Gd, is also supported by the XANES spectra. Efforts at stabilizing the oxygen conducting $Fm-3m$ phase in CeO₂-Gd₂O₃ solid solutions should therefore concentrate on tailoring the local environment of the Ce ion. We further suggest that our data may provide an explanation for the recently discovered giant electrostriction effect in Ce_{0.8}Gd_{0.2}O_{1.9}. Since this composition is at the limit of stability of the fluorite phase, local distortions in Ce_{0.8}Gd_{0.2}O_{1.9} may be modulated by an external electric field more readily than those of the other solid solutions.

DOI: [10.1103/PhysRevB.87.054101](https://doi.org/10.1103/PhysRevB.87.054101)

PACS number(s): 61.05.cj, 61.72.jd, 82.47.Ed

I. INTRODUCTION

Stabilization of the particular phase of a solid solution possessing optimal thermal, mechanical, or electrical properties is a challenge relevant to a wide variety of materials ranging from ion conductors to ferroelectrics. The CeO₂-Gd₂O₃ solid solution has been the subject of numerous structural studies^{1,2} motivated by the fact that Gd-doped ceria is one of the most important oxygen ion conductors for solid oxide fuel cells (SOFC). Introduction of Gd³⁺ into the Ce⁴⁺ sites of the CeO₂ lattice creates oxygen vacancies which are responsible for the high oxygen conductivity at temperatures above 500 °C. At low doping levels, the conductivity initially increases with Gd content. However, with addition of ~20 mol% Gd, it reaches a maximum and then decreases^{1,2} as the solid solution transforms from the initial fluorite ($Fm-3m$) phase of CeO₂ to the $Ia-3$ phase which is characteristic of Gd₂O₃.

The progression of intermediate states along the pathway from the $Fm-3m$ phase to the $Ia-3$ phase has been the subject of both experimental and theoretical arguments. Studies based on electron microscope measurements have reported that the Gd ions segregate and form C-type (i.e., Gd₂O₃-like, $Ia-3$ space group)³⁻⁵ nanosized clusters or microdomains,^{3,6-8} while the bulk of the material remains in the $Fm-3m$ phase. According to this view, the proliferation of such clusters eventually leads to the phase change. Grover *et al.*⁹ used Rietveld refinement of powder x-ray diffraction (XRD) data to solve the structure of CeO₂-Gd₂O₃ mixtures with 60 and 80 mol% Gd. Their work showed that for both the space group is $Ia-3$. There are two nonequivalent cation sites with different cation-oxygen bond lengths. The O1 (48e) oxygen sites are almost fully occupied (94%–95%), while the O2 sites (16c) are partially occupied.⁹ Due to the partial occupancy of the O2 anion site, the average cation coordination number lies between six and eight. Using Raman spectroscopy, the same group¹⁰ also suggested that the $Ia-3$ phase first appears between 20 and 30 mol% Gd.

A recently published synchrotron x-ray diffraction study¹¹ of the complete range of CeO₂-Gd₂O₃ solid solutions is consistent with the findings of Refs. 9 and 10. Artini *et al.*¹¹ have provided a set of model atomic structures based on Rietveld refinement of their diffraction data. Except for the pure ceria sample, the solid solutions are described by double fluorite symmetry, an important feature of which is a shift of the type 1 cation away from the fluorite position. Such a shift has been detected by the authors of Ref. 11 at a Gd doping level >20 mol%. In addition, a decrease in the occupancy of the O2 site, which is the signature of vacancy ordering, has been detected at >10 mol% Gd. However, as is well known, x-ray diffraction (XRD) provides only an averaged structure. It cannot distinguish between Ce and Gd ions; the cation sites in the Rietveld description of the $Ia-3$ structures are occupied randomly by Ce and Gd, with occupancy weighted by molar fraction. Consequently, XRD cannot quantify the distribution of oxygen vacancies about either of the cations. Recently, extended x-ray absorption fine structure (EXAFS) analysis, characterizing the local environment of the Ce and Gd ions in Ce_{0.8}Gd_{0.2}O_{1.9}, have shown that the oxygen vacancies clearly prefer Ce rather than Gd nearest neighbors.¹²⁻¹⁴ This preference has been attributed to the fact that Gd³⁺ ions are larger than Ce⁴⁺ and it is consistent with both the NMR data that show that vacancies are attracted to cation dopants that are smaller than the host ions¹⁵ and with theoretical modeling.¹⁶ Furthermore, it has been shown that, even though the XRD pattern of Ce_{0.8}Gd_{0.2}O_{1.9} does not display any diffraction peaks not consistent with $Fm-3m$ symmetry, the individual EXAFS-derived bond lengths, Ce-O and Gd-O, do not agree with the average Ce-O and Gd-O distances derived from the XRD analysis. This implies that the lattice undergoes local, uncorrelated distortions and, as a result, the local structure is different from the average.^{12,17} In the current work, we report results obtained by extending the x-ray absorption measurements to include the complete range of solid solutions. We present data and analysis of the Ce and Gd L_{III} edge

absorption spectra as obtained by EXAFS and x-ray absorption near edge structure (XANES) spectroscopies. We find that the double fluorite $Ia-3$ phase appears abruptly upon addition of 20–25 mol% Gd, and that it is related to changes in the local environment of Ce rather than of Gd.

II. EXPERIMENT AND DATA ANALYSIS

The powders of $Ce_{1-x}Gd_xO_{2-x/2}$, $x = 0.05-0.85$, used for these studies, were prepared by direct solid state synthesis with three subsequent cycles of regrinding, repelleting, and annealing at 1673 K for 48 h.⁹ We particularly note that these procedures are critical for maximizing sample homogeneity and crystallinity. In their absence, the observed phase composition and unit cell dimensions may not be reproducible.¹⁸ The pellets were slowly cooled to room temperature in the oven (>10 h) in order to ensure that no oxygen deficiency arose¹⁸ and that the resulting powders are representative of the corresponding stoichiometric phases. X-ray diffraction patterns were acquired with an Ultima III theta-theta powder diffractometer (Rigaku, Japan) at least three months after sample preparation to ensure that the unit cell had reached equilibrium value.¹⁹ The powders were measured in $\Theta-2\Theta$ mode with step size of 0.02° and rotation of >1 revolution per step in order to avoid the influence of texture. According to the diffraction patterns, the impurity content is limited to $\leq 1\%$. This is sufficiently low for impurities not to influence the results of the EXAFS and XANES measurements.

The EXAFS measurements were performed on the X18B beam line of the National Synchrotron Light Source at Brookhaven National Laboratory. L_{III} -edge spectra of Ce and Gd were acquired in transmission mode from powders prepared as described above and brushed over adhesive tape folded several times for uniformity. Representative, edge-step normalized EXAFS data for Ce and Gd L_{III} edges are shown in Fig. 1. The useful data ranges were limited by the Ce L_{II} and Gd L_{II} edges.

The EXAFS spectra were analyzed by nonlinear least square fits of FEFF6 theory²⁰ to the data using the Artemis program²¹ from the IFEFFIT data analysis package.^{22,23} Figures 2(a) and 2(b) show representative fits of Ce and Gd EXAFS spectra. Theoretical photoelectron scattering amplitudes and phase shifts were calculated for the model structures corresponding to CeO_2 and Gd_2O_3 , respectively. Passive electron reduction factors (S_0^2) were obtained from the fits to their respective bulk compounds (0.59 for the Ce L_{III} edge and 0.85 for the Gd L_{III} edge) and then kept constant in the fits for all the solid solutions. For the Ce L_{III} edge, the k range used for the fitting procedure was from 1.4 to 9.0 \AA^{-1} and the r range was from 1.4 to 2.2 \AA , which corresponds to six independent data points.²⁴ For the Gd edge, the number of independent data points was larger (seven), due to the larger k range (from 1.4 to 11 \AA^{-1}). Fitting parameters included the following: the correction to the bulk bond lengths; the disorder in the bond lengths, also known as the EXAFS Debye-Waller factors; as well as the correction ΔE that accounts for the different origins of the photoelectron energy between the experimental data and FEFF6 calculations. Bond lengths of the first nearest neighbors (Ce-O, Gd-O) were determined using a model which assumes a coordination number equal

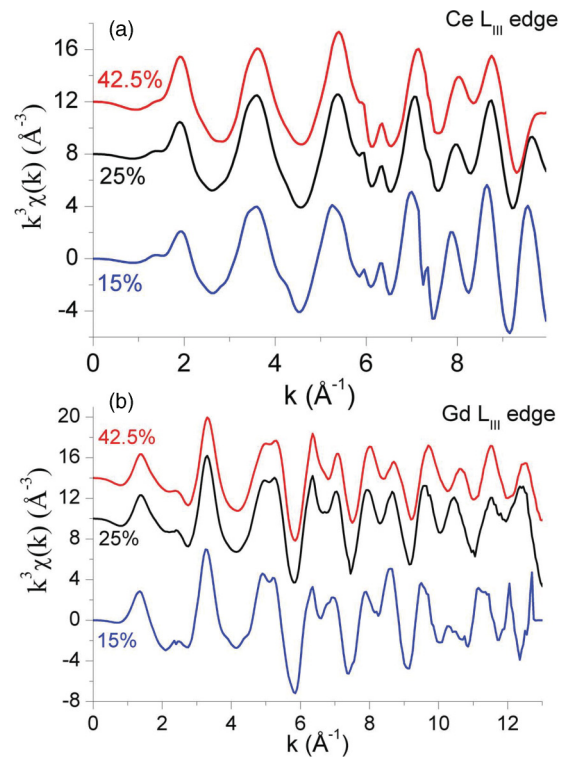


FIG. 1. (Color online) k^3 -weighted Ce L_{III} -edge (a) and Gd L_{III} -edge (b) EXAFS data shown for Gd concentrations below (15 mol%) and above (25 and 42.5 mol%) the structural phase transition.

to 8 for both Ce and Gd. As noted above, in the series of CeO_2 - Gd_2O_3 solid solutions, the number of nearest neighbor oxygen ions for each cation may vary from six to eight. Our assumption of eight neighbors affects the amplitude of the EXAFS signal, but not its phase, and therefore has no effect on the derived bond length. Only the first coordination shell was fitted in the current study since we showed previously^{12,25} that the nearest neighbor environment responds the most strongly to a change in the number of oxygen vacancies. The first coordination shell distances for pure CeO_2 and Gd_2O_3 are taken from a previous report.¹² For final fitting, only the corrections to the bulk bond lengths were varied, while the rest of the parameters remained fixed. The values of ΔE were fixed to be the same for all compositions (7.65 eV for Ce edge and 1.9 eV for Gd edge). The best values of the Debye-Waller factors were between 0.008 and 0.01 \AA^2 , depending on the edge.

III. RESULTS AND DISCUSSION

The XRD patterns of the $Ce_{1-x}Gd_xO_{2-x/2}$ powders, $x \leq 0.2$, can be indexed according to space group $Fm-3m$ [Figs. 3(a) and 3(b)]. The lattice constant is an increasing function of the doping level [Fig. 3(c)], as expected due, in part, to the larger ionic radius of the Gd ion. Already for $x \geq 0.25$, additional sharp peaks, indicating the formation of a superlattice with doubled lattice constant, are observed [Fig. 3(b)]. This also agrees with Ref. 11 and the earlier reported Raman spectroscopy.⁴ The lattice constant reaches a maximum at $x = 0.25$ and then monotonically decreases [Fig. 3(c)]. Some small differences in the lattice parameters

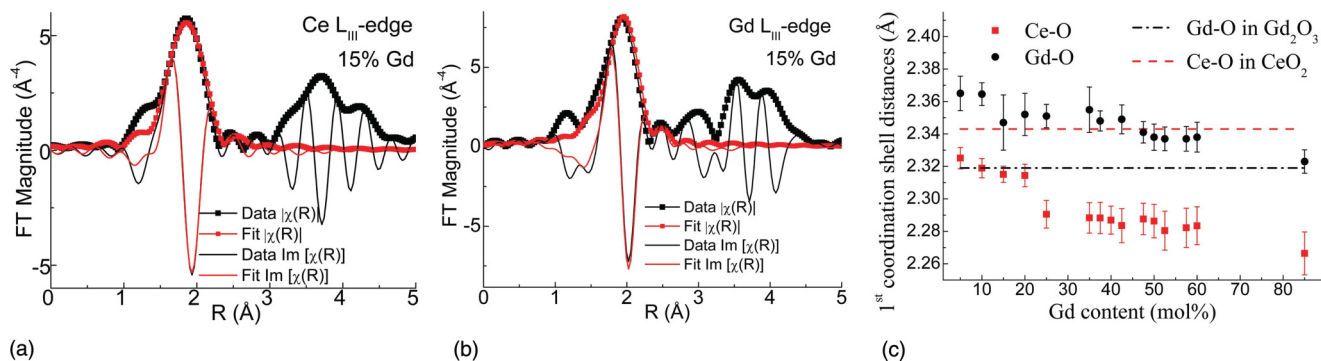


FIG. 2. (Color online) Best fits to the k^3 -weighted EXAFS data in R space at the Ce (a) and Gd (b) L_{III} edges in the compound with 15 mol% Gd. Shown are both the amplitude and the imaginary parts of the Fourier transforms of the data and the fits. (c) Average cation-oxygen distances in the first coordination shell as determined from EXAFS. Gd-O bond lengths decrease gradually with Gd concentration, whereas Ce-O bond lengths decrease abruptly between 20 mol% and 25 mol% Gd. The values of the first coordination shell distance for pure CeO_2 and Gd_2O_3 are taken from Ref. 12.

between our work and Ref. 11 may be attributed to the fact that the lattice parameter of Gd-doped ceria in the vicinity of 20 mol% of Gd depends on the sample history and may require up to three months to reach a constant value.¹⁹

Characteristic k^3 -weighted Ce L_{III} -edge [Fig. 1(a)] and Gd L_{III} -edge [Fig. 1(b)] EXAFS data are shown for Gd concentrations both below (15 at. %) and above (25 and 42.5 at. %) the structural phase transition. The best fit structural parameters obtained with IFEFFIT software are reported with 95% confidence limits. Local structural changes taking place during the $Fm-3m$ to $Ia-3$ phase transformation were

identified from the Gd-O and Ce-O bond lengths obtained by EXAFS data analysis (Fig. 2). While the Gd-O bond length decreases gradually from 2.365 \AA to 2.325 \AA over the entire range of Gd content measured, approaching the value observed for Gd_2O_3 ,¹² the average Ce-O bond length, initially 2.343 \AA in pure ceria, shows an abrupt decrease to 2.291 \AA between $x = 0.2$ and 0.25, i.e., coinciding with the onset of the characteristic diffraction of the $Ia-3$ phase. At higher Gd concentrations, the Ce-O bond length decreases gradually to 2.265 \AA at 85 mol% Gd. In the $Ia-3$ phase of Gd doped ceria, the first coordination shells are distorted but they are ordered

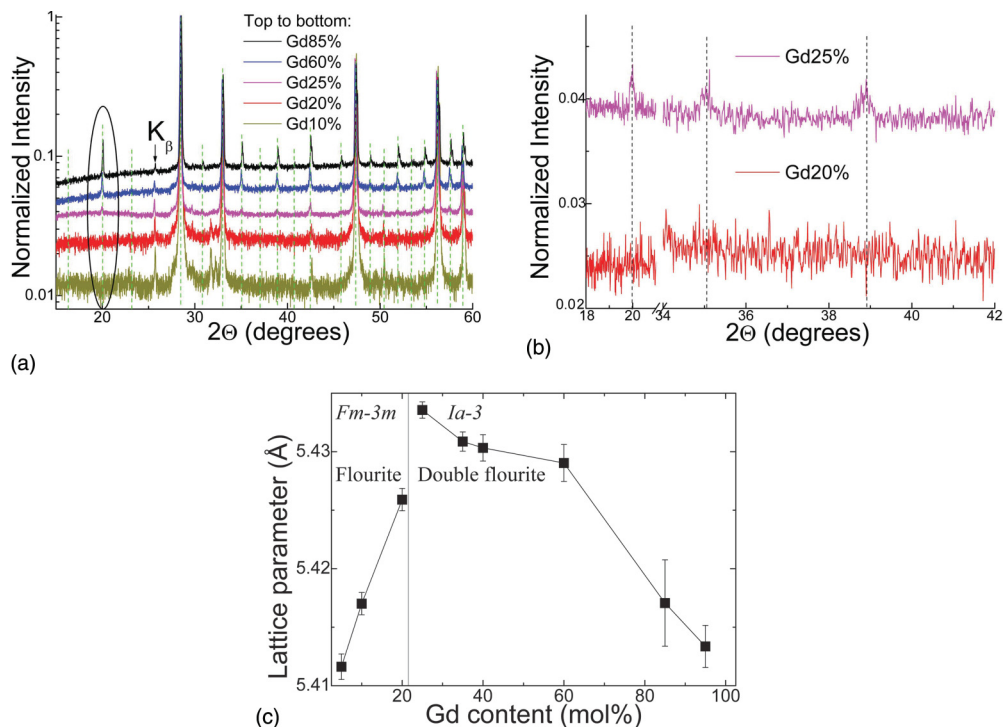


FIG. 3. (Color online) (a) Powder x-ray diffraction patterns of $Ce_{1-x}Gd_xO_{2-x/2}$, $x = 0.10-0.85$. The patterns for $x = 0.10$ and 0.20 identify the structure as $Fm-3m$. (b) Additional weak peaks, which appear when $x \geq 0.25$, correspond to the $Ia-3$ phase (vertical lines denote peak positions from C3.cif).¹¹ (c) Dependence of the lattice parameter as a function of Gd concentration. Since the $Ia-3$ phase forms with a doubling of the unit cell dimensions of the $Fm-3m$ phase, the lattice parameter/2 is plotted in the figure for Gd > 20 mol%.

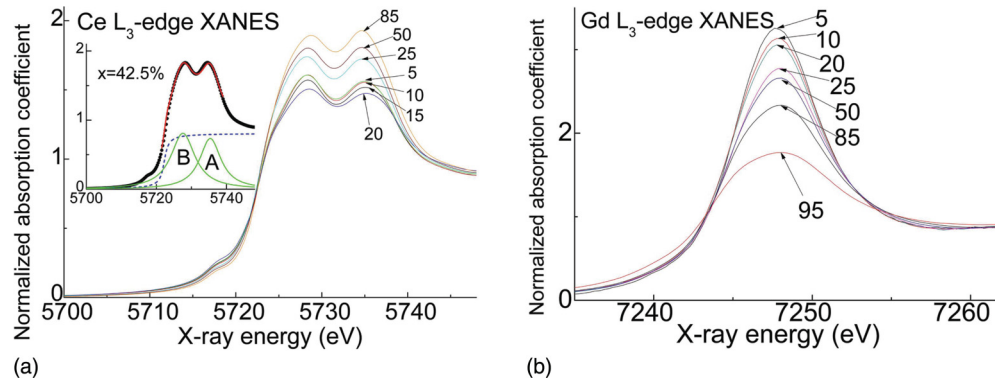


FIG. 4. (Color online) XANES spectra of (a) Ce L_{III} edge for Gd doping levels between 5 and 85 mol% and (b) Gd L_{III} edge for Gd doping levels between 5 and 95 mol%. The inset in (a) shows the deconvolution procedure used to determine the relative areas of peak A ($2\bar{p} f^{0.5d}$ state) and peak B ($2\bar{p} f^{1.5d} * \bar{L}$ state). $2\bar{p}$ denotes the empty state in the $2p$ shell and \bar{L} denotes an empty state in the neighboring oxygen orbital. The decrease in intensity of the Gd white line (b) is consistent with a decrease in the coordination number of the Gd ion.

with respect to the distribution of the oxygen vacancies.⁹ The different behavior of the two types of bonds in a solid solution are evidence for local deviation from the average structure that, according to the XRD data, is dominated by the transition from the fluorite to double fluorite phase. Since the vacancies are known to prefer smaller ions, Ce^{4+} in the case under consideration,^{12–14} the observed abrupt changes in the Ce-O bond length should be viewed as an indication of an abrupt change in the occupancy of the O2 site in the $Ia-3$ lattice. The decrease in the average Ce-O bond length in the fluorite phase upon increase in the vacancy concentration provides additional support for the earlier hypothesis^{25,26} that local distortions in the oxygen sublattice surrounding the Ce ions are similar to those found for the cation-1 site in the more heavily Gd-doped $Ia-3$ lattice.⁹ The initially cubic oxygen environment elongates along the body diagonal in the direction containing the vacancy and the six oxygen ions off this diagonal move closer to the Ce ion (see Fig. 1 in Ref. 26). The driving force for the local distortions is difficult to determine, in part because the lattice constant (Fig. 3) also increases abruptly between 20 and 25 mol% Gd concentration. A similar lack of correlation has been observed for the lattice constant and cation-oxygen distances in oxygen deficient $CeO_{2-\delta}$, $\delta = 0.05-0.1$.²⁵ The ionic radius of Ce^{3+} is more than 10% larger than that of Ce^{4+} . Apparently, lattice contraction due to the appearance of oxygen vacancies cannot compensate for the increase in the lattice constant resulting from the increase in the cation radius and local distortions. This effect has been analyzed by molecular dynamics simulation in Ref. 27.

The XANES spectra (Fig. 4) also demonstrate that the $Fm-3m$ to $Ia-3$ transition is associated with changes in the local environment of Ce rather than of Gd. The intensity of the Gd L_{III} -edge white line decreases monotonically with Gd content [Fig. 4(b) and Fig. 5], which is consistent with a uniform reduction in coordination number. The XANES spectra for the Ce L_{III} edge [Fig. 4(a)] are more complex. (1) The Ce L_{III} -edge white line comprises two peaks [Fig. 4(a), inset]: A ($2\bar{p} f^{0.5d}$ state) and B ($2\bar{p} f^{1.5d} * \bar{L}$ state),^{28–31} where $2\bar{p}$ denotes the empty state in the $2p$ shell and \bar{L} denotes an empty state in the oxygen orbital. Since the appearance of peak B originates from the transfer of charge from the oxygen to the Ce $4f$ orbital,³² the relative decrease in the intensity

of peak B with increased doping (Fig. 5, inset) should be attributed to the larger concentration of oxygen vacancies around Ce. (2) In the $Fm-3m$ region, the combined Ce L_{III} -edge peak intensity decreases with Gd content (Fig. 4 and Fig. 5). This is consistent with an increase in the concentration of vacancies introduced by Gd doping. However, the intensity increases abruptly with the appearance of the $Ia-3$ phase and then increases linearly with increasing Gd content. This marked change in the local environment of the Ce ion may be related to the fact that oxygen sites that are equivalent in the fluorite phase become nonequivalent in the $Ia-3$ phase and/or to the increased ordering of the near neighbor oxygen vacancies which accompany increased levels of Gd doping.⁹

We note that the inelastic behavior of Gd doped ceria, attributed to the local lattice distortions, is a strong function of temperature. For example, with 20 mol% Gd, elastic behavior is recovered upon heating to temperatures above 250 °C.¹⁹ Therefore, in the range of Gd concentrations in the vicinity of the phase transition (20–25 mol% Gd), one may expect that heating/cooling will have a modulating effect on the transformation to the $Ia-3$ phase.

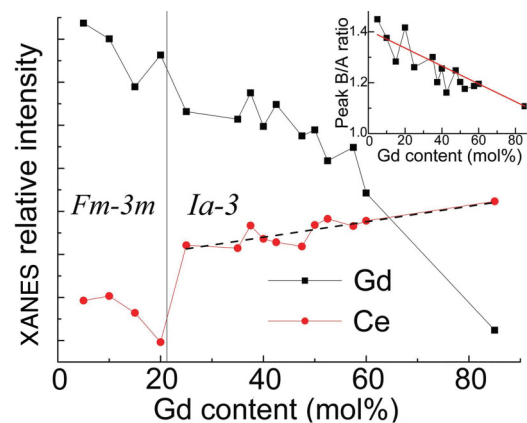


FIG. 5. (Color online) Main panel: relative areas of the main Ce and Gd L_{III} -edge peaks as a function of Gd content. Inset: the ratio of the areas of the B and A peaks. The vertical line marks the first appearance of XRD peaks characteristic of the $Ia-3$ phase.

IV. CONCLUSIONS

On the basis of the analysis of EXAFS and XANES data, three important conclusions may be drawn.

(1) X-ray diffraction from specially prepared and fully equilibrated bulk powder samples of $\text{Ce}_{1-x}\text{Gd}_x\text{O}_{2-x/2}$, $x = 0.05-0.85$ detects the $Fm-3m$ to $Ia-3$ phase transformation between $x = 0.2$ and $x = 0.25$, coinciding with a maximum in the unit cell dimension.

(2) By measuring EXAFS and XANES spectra on the same samples of $\text{CeO}_2/\text{Gd}_2\text{O}_3$ solid solutions, we have successfully identified differences in the changing environments of the Ce and Gd ions as a function of Gd doping. We relate the onset of the $Fm-3m \rightarrow Ia-3$ phase transformation to an abrupt reorganization of the local environment of Ce, whereas that of Gd changes gradually. Therefore, we suggest that efforts to stabilize the $Fm-3m$ phase, in order to enhance conductivity, should focus on modifying the local environment of Ce. Oxygen vacancies are known to prefer Ce over Gd^{12,25} because the former has the smaller ionic radius. In this view, one could suggest that codoping of Gd-doped ceria with trivalent dopants that have a smaller ionic radius (Y or Sm) than that of Ce^{4+} and

therefore attract oxygen vacancies^{13,16} may widen the stability range of the $Fm-3m$ phase.

(3) Since $\text{Ce}_{0.8}\text{Gd}_{0.2}\text{O}_{1.9}$ is near the limit of stability of the fluorite phase, local distortions may be modulated by an external electric field more readily than in any of the other solid solutions and thereby may lead to the recently observed giant electrostriction effect.²⁶

ACKNOWLEDGMENTS

I.L. wishes to thank the US-Israel Binational Science Foundation for funding this research. I.L. also wishes to acknowledge the assistance of the Nancy and Stephen Grand Research Center for Sensors and Security. R.K. acknowledges the Professor R. Rahamimoff Travel Grant Program of the US-Israel Binational Science Foundation. The research is also made possible in part by the generosity of the Harold Perlman Family. A.I.F. acknowledges the support of this work by the US Department of Energy (DOE) Grant No. DE-FG02-03ER15476. X18B beamline is supported, in part, by Synchrotron Catalysis Consortium (US DOE Grant No. DE-FG02-05ER15688).

*Currently at the Science Institute, University of Iceland, Reykjavik, Iceland.

†frenkel@bnl.gov

‡igor.lubomirsky@weizmann.ac.il

¹M. Mogensen, N. M. Sammes, and G. A. Tompsett, *Solid State Ionics* **129**, 63 (2000).

²H. Inaba and H. Tagawa, *Solid State Ionics* **83**, 1 (1996).

³Z. P. Li, T. Mori, F. Ye, D. R. Ou, J. Zou, and J. Drennan, *Phys. Rev. B* **84**, 180201 (2011).

⁴H. Inaba, R. Sagawa, H. Hayashi, and K. Kawamura, *Solid State Ionics* **122**, 95 (1999).

⁵T. Ohashi, S. Yamazaki, T. Tokunaga, Y. Arita, T. Matsui, T. Harami, and K. Kobayashi, *Solid State Ionics* **113**, 559 (1998).

⁶Z. P. Li, T. Mori, F. Ye, D. R. Ou, J. Zou, and J. Drennan, *J. Chem. Phys.* **134**, 224708 (2011).

⁷Z. P. Li, T. Mori, F. Ye, D. R. Ou, J. Zou, and J. Drennan, *Microsc. Microanal.* **17**, 49 (2011).

⁸F. Ye, T. Mori, D. R. Ou, J. Zou, and J. Drennan, *Solid State Ionics* **180**, 1414 (2009).

⁹V. Grover, S. N. Achary, and A. K. Tyagi, *J. Appl. Crystallogr.* **36**, 1082 (2003).

¹⁰A. Banerji, V. Grover, V. Sathe, S. K. Deb, and A. K. Tyagi, *Solid State Commun.* **149**, 1689 (2009).

¹¹C. Artini, G. Costa, M. Pani, A. Lausi, and J. Plaisier, *J. Solid State Chem.* **190**, 24 (2012).

¹²A. Kossoy, A. I. Frenkel, Q. Wang, E. Wachtel, and I. Lubomirsky, *Adv. Mater.* **22**, 1659 (2010).

¹³H. Deguchi, H. Yoshida, T. Inagaki, and M. Horiuchi, *Solid State Ionics* **176**, 1817 (2005).

¹⁴S. Yamazaki, T. Matsui, T. Ohashi, and Y. Arita, *Solid State Ionics* **136**, 913 (2000).

¹⁵S. Sen, H. J. Avila-Paredes, and S. Kim, *J. Mater. Chem.* **18**, 3915 (2008).

¹⁶X. Wei, W. Pan, L. F. Cheng, and B. Li, *Solid State Ionics* **180**, 13 (2009).

¹⁷A. Frenkel, E. A. Stern, A. Voronel, M. Qian, and M. Newville, *Phys. Rev. Lett.* **71**, 3485 (1993).

¹⁸I. Riess, R. Koerner, M. Ricken, and J. Noeltling, *Solid State Ionics* **28**, 539 (1988).

¹⁹A. Kossoy, Y. Feldman, R. Korobko, E. Wachtel, I. Lubomirsky, and J. Maier, *Adv. Funct. Mater.* **19**, 634 (2009).

²⁰S. I. Zabinsky, J. J. Rehr, A. Ankudinov, R. C. Albers, and M. J. Eller, *Phys. Rev. B* **52**, 2995 (1995).

²¹B. Ravel and M. Newville, *J. Synchrotron Radiat.* **12**, 537 (2005).

²²M. Newville, *J. Synchrotron Radiat.* **8**, 96 (2001).

²³M. Newville, *J. Synchrotron Radiat.* **8**, 322 (2001).

²⁴E. A. Stern, *Phys. Rev. B* **48**, 9825 (1993).

²⁵A. Kossoy, A. I. Frenkel, Y. Feldman, E. Wachtel, A. Milner, and I. Lubomirsky, *Solid State Ionics* **181**, 1473 (2010).

²⁶R. Korobko, A. Patlolla, A. Kossoy, E. Wachtel, H. L. Tuller, A. I. Frenkel, and I. Lubomirsky, *Adv. Mater.* **24**, 5857 (2012).

²⁷D. Marrocchelli, S. R. Bishop, H. L. Tuller, and B. Yildiz, *Adv. Funct. Mater.* **22**, 1958 (2012).

²⁸Y. Takahashi, H. Shimizu, A. Usui, H. Kagi, and M. Nomura, *Geochim. Cosmochim. Acta* **64**, 2929 (2000).

²⁹F. Zhang, P. Wang, J. Koberstein, S. Khalid, and S. W. Chan, *Surf. Sci.* **563**, 74 (2004).

³⁰A. V. Chadwick and S. L. P. Savin, *J. Alloys Compd.* **488**, 1 (2009).

³¹A. V. Soldatov, T. S. Ivanchenko, S. Dellalonga, A. Kotani, Y. Iwamoto, and A. Bianconi, *Phys. Rev. B* **50**, 5074 (1994).

³²A. Bianconi, A. Marcelli, H. Dexpert, R. Karnatak, A. Kotani, T. Jo, and J. Petiau, *Phys. Rev. B* **35**, 806 (1987).